Nanotechnology

PAPER

# The enhanced photocatalytic performance of $SnS_2$@$MoS_2$ QDs with highly-efficient charge transfer and visible light utilization for selective reduction of mythlen-blue

To cite this article: Gomaa Khabiri *et al* 2020 *Nanotechnology* **31** 475602



IOP Publishing Nanotechnology

Nanotechnology **31** (2020) 475602 (9pp) https://doi.org/10.1088/1361-6528/aba212

# The enhanced photocatalytic performance of $SnS_2$@$MoS_2$ QDs with highly-efficient charge transfer and visible light utilization for selective reduction of mythlen-blue

**Gomaa Khabiri[1,2], Abdelaziz M. Aboraia[1,3], S Omar[1], Malak Soliman[1], Asmaa M.A. Omar[2], Mikhail V Kirichkov[1] and A V Soldatov[1]**

[1] Smart Materials Research Institute, Southern Federal University, Sladkova 178/24, 344090, Rostov-on-Don, Russia
[2] Physics Department, Center for Environmental and Smart Technology (CEST), Faculty of Science, Fayoum University, Fayoum 63514, Egypt
[3] Department of Physics, Faculty of Science, Al-Azhar University, Assiut 71542, Egypt

E-mail: gma01@fayoum.edu.eg and a.m.aboraia@gmail.com

Received 29 April 2020, revised 24 June 2020
Accepted for publication 2 July 2020
Published 31 August 2020

**Abstract**

Molybdenum disulfide ($MoS_2$) has recently been considered as an effective material for potential photocatalytic applications; however, its photocatalytic activity was limited due to the low density of active sites. In this work, $MoS_2$ Quantum dots (QDs) were synthesized via the ultrasonication technique to construct heterostructure with $SnS_2$ nanosheets ($SnS_2$@$MoS_2$ QDs) and the prepared materials were tested for photocatalytic applications for Methylene blue (MB). Pristine $SnS_2$ and $SnS_2$@$MoS_2$ QDs nanocomposite were analyzed by XRD, TEM, PL, and Uv–Vis. Both $SnS_2$ and $SnS_2$@$MoS_2$ QDs exhibited a single trigonal phase with the P-3m1 space group. The TEM analysis confirmed the coupling between the pristine $SnS_2$ and $SnS_2$@$MoS_2$ QDs. The results of photocatalytic activity toward MB indicated that $SnS_2$@$MoS_2$ QDs material exhibits much superior photocatalytic performance compared to pristine $SnS_2$. The excellent photodegradation performance of $SnS_2$@$MoS_2$ QDs is due in the main to the formation of heterojunction between $SnS_2$ and $MoS_2$ QDs with narrow bandgap formation, which results in a facile carriers transfer and thus high photocatalytic efficiency. A representative mechanism of the photodegradation for $SnS_2$@$MoS_2$ QDs photocatalyst was proposed. Such an ultrasonic technique is capable of producing small metallic particle size that can be used to construct new heterostructures for water remediation applications.

Supplementary material for this article is available online

Keywords: $SnS_2$, hydrothermal, ultrasonication, methylene blue, $MoS_2$ QDs, $SnS_2$@$MoS_2$ QDs photocatalyst

(Some figures may appear in colour only in the online journal)

 

## 1. Introduction

Particular attention has recently been paid to environmental contamination, such as toxic pollutants and organic compounds released by chemical industries, which are extremely hazardous to the environment [1–3]. Organic dyes such as Methylene blue (MB), Rhodamine B (RhB), and Methyl orange (MO) are a category of traditional pollutants that poses serious concerns on human health and animals. Pollution of water with these organic dyes is considered to be the most harmful threats to sustaining life. Therefore, many approaches have been proposed to treat pollutant water, including biodegradation [4], chemical oxidation [5], membrane separation [6], photocatalysis [7] and adsorption [8]. Among them, photocatalysis offers good potential for the removal of such organic contamination [9, 10]. This is because the other approaches surfer from some broblems such as low product, high-pressure and energy conditions and high pollution.

Semiconductor photocatalysis is a promising friendly technique for removing aqueous organic dyes via utilizing natural sunlight or artificial lighting. As a potential photocatalyst, Tin disulfide ($SnS_2$) has recently become one of the most important metal-sulfide materials, due to its unique layered stricture, which has a hexagonal structure with densely packed tin atoms sandwiched between two sulfur atoms [11]. It has the advantages of good stability, non-poisonous, low cost, high ratio of solar usage (high optical absorption coefficient >104 $cm^{-1}$), and thermal air stability [12, 13]. Although, $SnS_2$ has been proven to be a visible photocatalyst for organic dyes due to its narrow bandgap ∼2.2 [13], however, its photocatalytic efficiency is limited by the rapid recombination of charge carriers. Up to the present time, there are few reports of its use as a photocatalyst.

The specific area of the ultra-thin layers of $SnS_2$ is high, making it ideal for constructing heterostructures with different materials to enhance their photocatalytic performance [14]. Earlier reports proved that the combining of $SnS_2$ with sulfides or oxides could provide new photocatalyst with high photocatalytic activity toward organic dyes and heavy metals [15–18]. The loading of co-catalyst on the semiconductor surface as a host catalyst can effectively improve the charge carrier mobility. Zhang, Jun, and co-works [14] claimed enhancement in the photocatalytic activity of the $SnS_2$/$MoS_2$ heterostructures, which can be ascribed to the improvement of the photoinduced carriers' separation and the good energy band matching. Another study of the photocatalytic activity on $SnS_2$/RGO nanocomposite revealed ∼99.7% Remazol Brilliant Blue R (RBB) and ∼97.0% Remazol Brilliant Red X (RBR) efficiency under irradiation for 2–3 h [17].

Over the last years, molybdenum disulfide ($MoS_2$) has been largely regarded as a potential co-catalyst, thanks to its low cost, high abundance, and unique properties, which are similar to noble metals [19]. $MoS_2$ can exist in stable semiconducting phase (2 H) and metastable metallic nature (1 T). Moreover, the coexistence of 1 T and 2 H domains in one layer of $MoS_2$ as a hybrid phase (1 T/2 H) was reported [20]. For photocatalytic and electrochemical applications, 2 H and 1 T-$MoS_2$ can be efficiently used as a photocatalyst, especially, 1 T-$MoS_2$ due to their high density of edges and basal plane active side and high conductivity [21]. $MoS_2$ quantum dots ($MoS_2$ QDs) gained more focus compared to bulk or nanosheets $MoS_2$ due to their high number of active edge atoms and good stability in aqueous solution [22]. It should be noted that most of the earlier reports centered on the 2 H-$MoS_2$ phase; however, due to its lower conductivity, the photocatalytic activity was limited. To the present time, there are only a few studies concerning 1 T-$MoS_2$ QDs [23]. Sun and co-authors [24] claimed an improvement in the $H_2$ generation when $MoS_2$ QDs loaded on CdS NRs, and they attributed the enhancement in the $H_2$ production to the high charge carrier mobility in the CdS NRs@$MoS_2$ QDs heterostructure.

Numerous approaches can be used to synthesize $MoS_2$ QDs, including hydrothermal [25], liquid exfoliation [26], and lithium intercalation [27]. Although, for the high content of 1 T-$MoS_2$ QDs, an increase in electrochemical hydrogen evolution reaction (HER) activity was achieved; however, the preparation required a complicated process and was time-consuming. Hence, developing an easy, effective, non-toxic, and one-step solution approach for synthesizing high concentration 1 T-$MoS_2$ QDs remains a challenge. Up to now, the micro/nanocomposites of $MoS_2$ and $SnS_2$ were prepared with micro or several nanometers-sized of $MoS_2$, to form heterostructures [14]. However, the poor contact between $SnS_2$ and $MoS_2$ results in a shorter lifetime of charge carriers and, thus, low photocatalytic activity. Therefore, our challenge in this work is to improve the photocatalytic performance of $SnS_2$ by designing a heterostructure of $SnS_2$@$MoS_2$ with low cost and facile technique.

So, in this work, we for the first time, focus on studying the effect of 1 T-$MoS_2$ $MoS_2$ QDs on the photocatalytic performance of $SnS_2$. The $SnS_2$@$MoS_2$ QDs nanocomposite was prepared by the ultrasonication method. The prepared $SnS_2$@$MoS_2$ QDs nanocomposite show significantly enhanced photodegradation toward methylene blue (MB) compared to pristine $SnS_2$ under light illumination. Additionally, a potential mechanism was suggested for the photocatalytic process of the $SnS_2$@$MoS_2$ QDs nanocomposites over MB. In summary, the $MoS_2$ QDs can provide more reactive sites for dye degradation and can present as an electron acceptor with high conductivity, thus leading to the superior photodegradation activity of $SnS_2$@$MoS_2$ QDs nanocomposite.

## 2. Experimental

### 2.1. Materials

Thiourea ($CH_4N_2$ S), Ammonium molybdate ($(NH_4)_2MoO_4$), and Tin(II) chloride ($SnCl_4.2H_2O$) were used as chemical reagents to prepare $MoS_2$ QDs and $SnS_2$ nanosheets. All chemicals were purchased from Sigma Aldrich without further purification.

### 2.2. Preparation of $SnS_2$

The $SnS_2$ structure was prepared by a solvothermal method using Isopropanol. Typically, 0.675 g of Tin chloride ($SnCl_4.5H_2O$) and 0.293 g of thiourea were dissolved in 38.5 ml of Isopropanol under stirring for several minutes. By using a filling ration of 77%, the solution was then transferred into 50 ml Teflon-lined stainless at 180 °C for 22 h. By deionized water and methanol, the obtained product was washed three times after cooling to room temperature. After drying at 80 °C for 12 h, the yellow powder was obtained.

### 2.3. Synthesis of $MoS_2$ QDs

To prepare $MoS_2$ QDs (Scheme 1), first, we prepare $MoS_2$ material through the hydrothermal method, according to literature [28] with some modifications. Mainly, 0.2785 g of thiourea and 0.9055 g of ammonium molybdate were mixed in 22 ml distilled water with stirring for 30 min. The mixture was moved to Teflon-lined stainless steel autoclave and at temperature 180° C for 20 h. After the mixture was cooled, the precipitate was then washed, centrifuged three times using distilled water and methanol, and then dried at 80° C for 12 h. Second, 50 mg of the prepared $MoS_2$ material was mixed with 50 ml of distilled water and sonicated for 2 h to obtain a high suspension. The suspension was then centrifuged for 90 min at 16 000 rpm, and then the $MoS_2$ QDs were obtained.

### 2.4. Synthesis of $SnS_2$@$MoS_2$ QDs nanocomposite

Utilizing ultrasonic mixing methods, the $SnS_2$@$MoS_2$ QDs nanocomposite was prepared (Scheme 2). We admixed 10 ml of $MoS_2$ QDs (0.004 g) and 50 mg of $SnS_2$. Then, the mixture was ultrasonicated for 2 h and then washed, centrifuged, and dried for 12 h at 60 ° C to obtain $SnS_2$@$MoS_2$ QDs material.

### 2.5. Photocatalytic experiment

Photocatalytic degradation of the as-prepared material was evaluated by the decomposition of MB (10 ppm) in an aqueous solution under right-light illumination by tungsten lamp. 25 mg of the photocatalyst was mixed with 50 ml 10 ppm dye solution and then stirred for several minutes in dark condition to achieve the adsorption-desorption equilibrium. After that, 3 ml of the mixture solution was taken out at different intervals and centrifuged for 10 min and then analyzed by UV–Vis spectrometer.

## 3. Result and discussion

$SnS_2$@$MoS_2$QDs nanocomposite has been synthesized by a simple ultrasonic technique for 2 h and was characterized to identify the influence of $MoS_2$ QDs on the crystal structure and the microstructure of the obtained materials. Figure 1. Displays the XRD diffraction of pure $SnS_2$ and $SnS_2$@$MoS_2$ QDs nanocomposite. Notably, the as-prepared $SnS_2$ proved that it contains a trigonal phase with a P-3m1 space group. The diffraction peaks at 15.2°, 28.33°, 41.82, 49.97°, 52.1°, 54.67°, and 60.97° correspond to the (001), (100), (011), (012), and (110), (111), (013) and (021) planes of $SnS_2$, respectively according to cryptographic open-source (code:9 000 613). The Rietveld refinement confirmed that there were no impurities with another phase since all peaks were a proper matching with $SnS_2$. The XRD pattern of $SnS_2$@$MoS_2$ QDs heterostructure confirmed that all indexed peaks are $SnS_2$ except the peak at 40.3° referred to $MoS_2$, as demonstrated in figure 1, revealing the successful formation of $SnS_2$@$MoS_2$ QDs. The absence of most $MoS_2$ peaks may be due to the low content of $MoS_2$ QDs in the $SnS_2$@$MoS_2$ QDs nanocomposite and the very small size of $MoS_2$ QDs, which cannot be identified by XRD [29].

**Table 1.** The lattice parameters of $SnS_2$ and $SnS_2$@$MoS_2$ QDs heterostructure.

| Samples | a (Å) | b (Å) | c (Å) | Volume (Å$^3$) |
|---|---|---|---|---|
| **$SnS_2$** | 3.62782 | 3.62782 | 5.90067 | 67.255 |
| **$SnS_2$@$MoS_2$ QDs** | 3.63622 | 3.63622 | 5.88525 | 67.390 |

Table 1 exhibited the crystal lattice parameters of $SnS_2$ before and after coating by $MoS_2$ QDs. One can see that the a and b lattice parameters increased for $SnS_2$@$MoS_2$ QDs, while the c lattice parameter decreased indicating the foemation of crystal defects after loading of $MoS_2$ QDs.

### 3.1. TEM characterization

The morphology and microstructure of the as-synthesized samples were studied by TEM at different magnifications, as demonstrated in figure 2. Evidently, $MoS_2$ QDs are distributed uniformly on very thin $MoS_2$ nanosheets without any noticeable agglomeration (figures 2(a) and (b)) with a size of around 3.5–9 nm and an average size of 4.68 nm (figure 2(c)). The coupling between $SnS_2$ and $MoS_2$ QDs was observed in figure 2(d). Obviously, the surface of $SnS_2$, which has a size of 120 to 150 nm, was coated by $MoS_2$ QDs with random distribution (The region surrounded by the white circle), revealing that the $MoS_2$ QDs retain their shape after combining with $SnS_2$. Hence, it is proven that the $MoS_2$ QDs are attached to the surface of $SnS_2$ with good interfacial contact. The construction of such structures is well suitable for charge carrier transmission, resulting in improvement of the photocatalytic performance.

### 3.2. Optical properties

Figure 3(a) displays the Ultraviolet-visible absorption spectra of the as-prepared materials. Obviously, there is an absorption ranged from 200 nm to 600 nm for both samples pristine $SnS_2$ and $SnS_2$@$MoS_2$ QDs material. Moreover, we noted that the absorption intensity of $SnS_2$@$MoS_2$ QDs is higher than $SnS_2$ due to the good contact between the $SnS_2$ and $MoS_2$. Arguably, the enhancement of the absorbance spectra of the nanocomposite material could be attributed to the modification in the energy band structure of the nanocomposite due to the construction of heterojunction between $SnS_2$ and $MoS_2$ [14]. In fact, many factors affect the semiconductor bandgap, for instance: the grain size, doping, and coating.

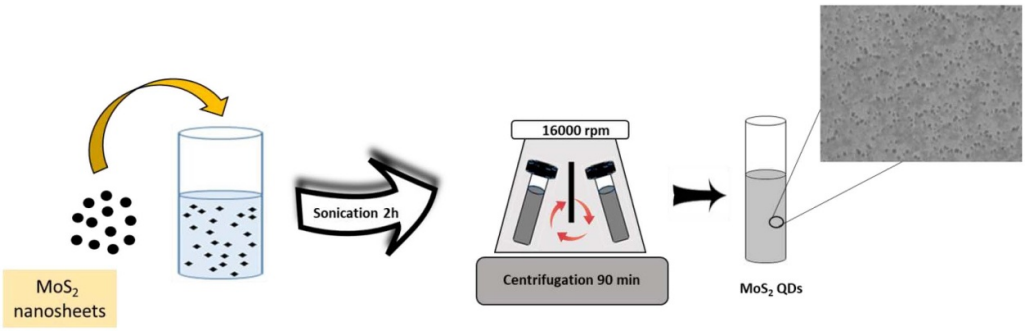


**Scheme 1.** Schematic representation of the synthetic route of $MoS_2$ QDs.


**Scheme 2.** Schematic representation of the synthetic route of $SnS_2$@$MoS_2$ QDs nanocomposite.

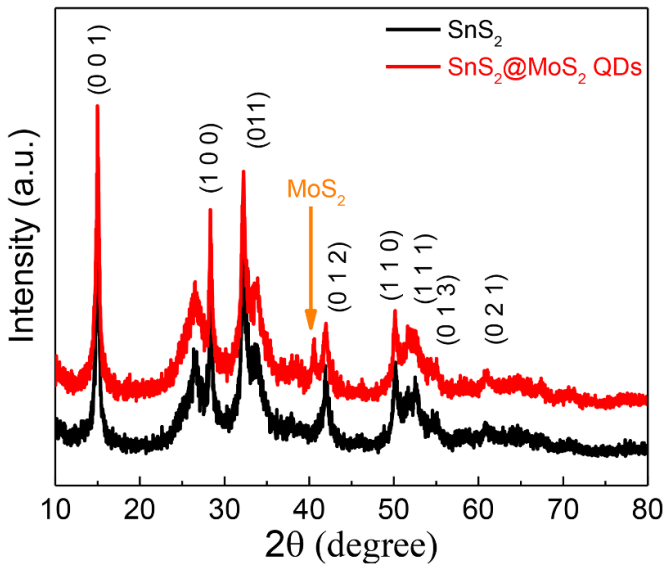


**Figure 1.** XRD patterns of pure $SnS_2$ and $SnS_2$@$MoS_2$ QDs nanocomposites.

Herein, there is no significant change in the grain-sized of pristine and $SnS_2$@$MoS_2$ QDs, as confirmed by XRD results (table 1). Thus, the coating of the $SnS_2$ surface by $MoS_2$ QDs has an essential role in the change of optical properties of the nanocomposite sample. In accordance with the optical absorption theory, we can determine the energy gap of the prepared materials based on the following relation [30]:

$$(\alpha.h\nu)^n = A\,(h\nu - E_g) \quad (1)$$

Where $\alpha$ is the absorption coefficient, hν (eV) is a photon-energy, A is the constant, *e.g.* (eV) is the optical bandgap, n is the exponential constant as-sociated with the transition form, with n = 2, 1/2 for a direct and indirect bandgap transition, correspondingly. To determine the energy gap of $MoS_2$ QDs, $SnS_2$, and $SnS_2$@$MoS_2$ QDs, we can plot the value of $(\alpha.h\nu)^2$ vs. hν, as shown in figure 3(b). The energy band gap was estimated to be 2.36 eV and 2.18 eV for $SnS_2$ and $SnS_2$@$MoS_2$ QDs, respectively, as shown in figures 5(a) and (b). The decrease of the energy gap of $SnS_2$ after coating by $MoS_2$ QDs maybe refer to the crystal defects created due to the introduction of $MoS_2$ QDs. Meanwhile, these defects occur shallow level donor impurities energy levels in the bandgap near the conduction band edge, and shallow acceptor impurities create energy levels near the valence band edge. For $MoS_2$ (figure 3(c)), the lack of any absorption bands indicates the metallic nature of the material [31]. The bandgap was estimates (inset figure 3(c)) and was found to be 1.94 eV, which is consistent with literature [32].

The spectrum of PL at room temperature for the prepared materials with an excitation wavelength of 390 nm is shown in figure 4. Both the samples exhibit two strong emission peaks

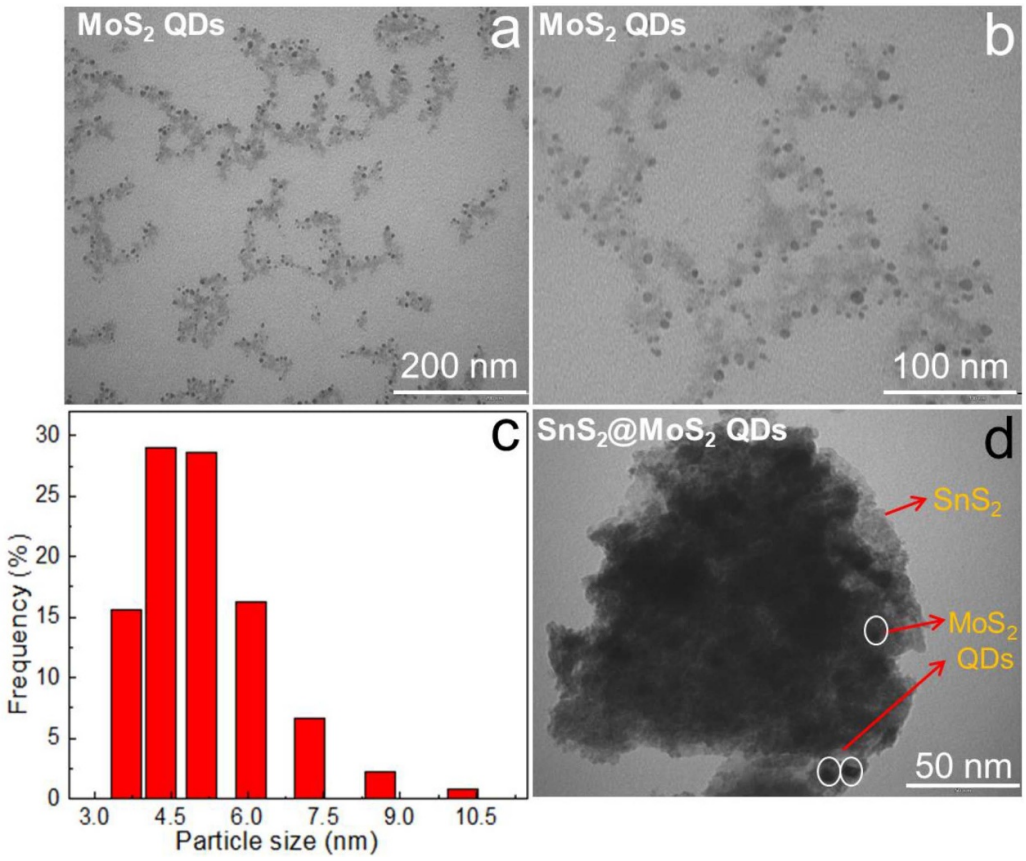


**Figure 2.** (a,b) TEM images of $MoS_2$ QDs, (c) the corresponding particle size and (d) TEM images of $SnS_2$@$MoS_2$ QDs nanocomposite.

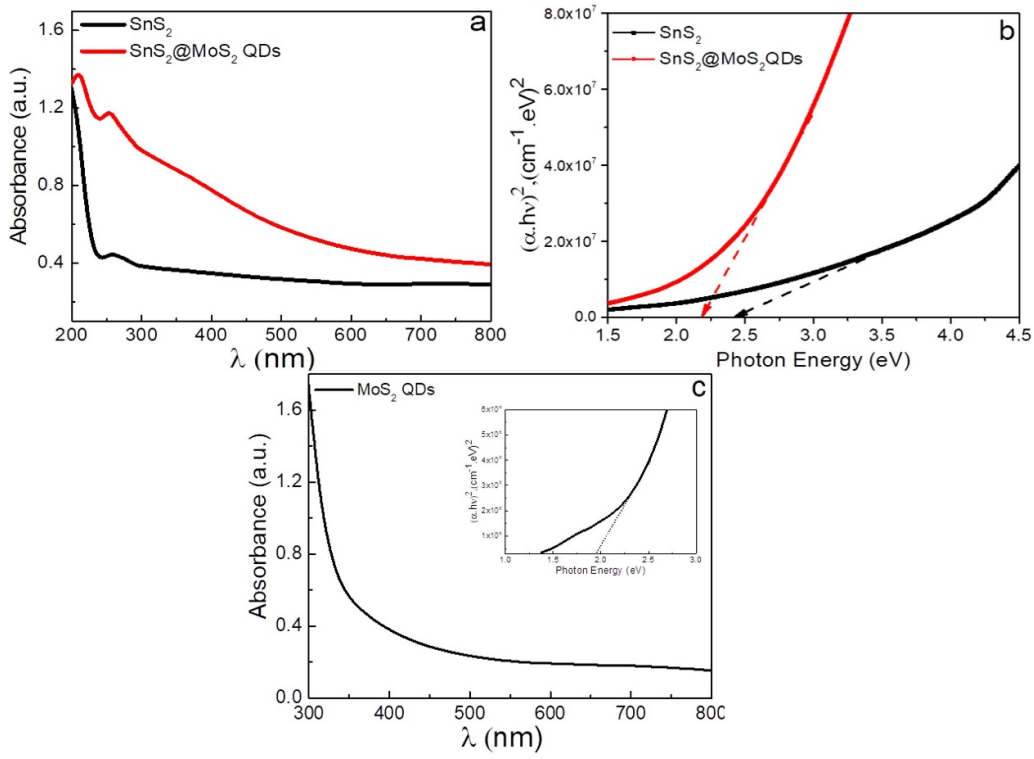


**Figure 3.** (a) Uv–Vis spectrum and (b) Energy bandgap of $SnS_2$, $SnS_2$ @$MoS_2$ materials, and (c) Uv–Vis of $MoS_2$ QDs. The inset figure is the calculated bandgap of $MoS_2$ QDs.

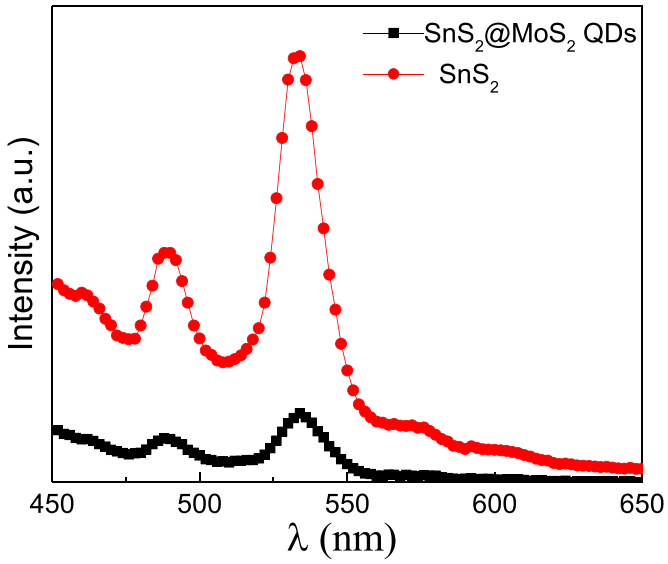


**Figure 4.** PL spectra of the pure $SnS_2$ nanosheets and $SnS_2$@$MoS_2$ QDs samples upon excitation by 390 nm at room temperature.

at 489 and 534 nm. Also, there is another peak at 460 nm, observed for pure $SnS_2$, which can be associated with the transition of trapped electrons from the donor-levels to the valence-band [33]. The observed emission peak at around 489 nm can originate from the radiation produced by the recombination of excitons' absorption that produced electrons which lie at higher excited energy levels [34]. Moreover, the emission peaks at 534 nm can be correlated with the emission of the quantum-confined $e^-/h^+$ pair recombination, which is slightly smaller in energy than the bandgap of nanocrystals [35]. The improved peaks intensity of the $SnS_2$@$MoS_2$ QDs may be attributed to the increased defects concentration induced by coating, which is dependable with the XRD results. Pristine $SnS_2$ exhibits a significant emission due to its high photoinduced carrier's recombination. By loading $MoS_2$ QDs on the $SnS_2$ surface, the emission intensity is surprisingly quenched, which means rapid electron transfer from $SnS_2$ nanosheets to $MoS_2$ QDs, resulting in lower $e^-/h^+$ recombination and thus improving the photodegradation activity.

### 3.3. Photocatalytic performance

The photocatalytic performance of the as-synthesized $SnS_2$ and $SnS_2$@$MoS_2$ QDs nanocomposites were evaluated by selective reduction of methylene blue under visible light irradiation. Figure 5(a) exhibits the pristine $SnS_2$ absorption spectra photocatalyst. The intensity of the absorption peak reduces with growing irradiation time, which indicates that the MB molecules were degraded with time. After 120 min, almost 75.0% of the MB got degraded. Figure SI (available at stacks.iop.org/NANO/31/475602/mmedia) shows that the $MoS_2$ QDs display low photocatalytic activity ((72.0%)) for MB within 120 min. Therefore, to enhance the performance of the photocatalyst, $SnS_2$ was coated by $MoS_2$ QDs, and the results of photodegradation activity are shown in figure 5(b). Notably, about 87.0% of MB dye was degraded after about 10 min, and after 120 min, the MB molecules were completely decomposed (figure 5(c)), indicating the superior photocatalytic performance of $SnS_2$@$MoS_2$ QDs material. The creation of a heterostructure with a proper contact is a key factor in improving the photocatalytic activity of the heterostructure material.

Our prepared material $SnS_2$@$MoS_2$ QDs has an excellent photocatalyst performance compared to the reported literature, as demonstrated in table 2. The excellent photodegradation performance of the $SnS_2$@$MoS_2$ QDs nanocomposite is essentially ascribed to the following explanations; (1) The high light absorption response of $SnS_2$@$MoS_2$ QDs material due to the introducing of $MoS_2$ QDs. The coupling of $MoS_2$ QDs and $SnS_2$ nanosheets as confirmed by TEM, narrowing the bandgap of the of $SnS_2$@$MoS_2$ QDs nanocomposites and thus, greatly increasing absorption in the visible light region; (2) The very small $MoS_2$ QDs with metallic nature can serve as active electron acceptors, providing more efficient paths for the photoexcited carriers to transfer between $MoS_2$ and $SnS_2$ in a short distance, resulting in a longer lifetime of the charge carriers and consequently, enhancing the photocatalytic efficiency.

For the detailed study of the photodegradation behavior of the prepared materials toward MB, the degradation kinetics was investigated using the first-order kinetic model, and second-order kinetic model according to equations (2) and (3), which is generally used for in the photocatalytic process if the primary concentration of pollutants is low [7, 42].

$$1/C = K_2^{/}t + 1/C_o \tag{2}$$

$$-ln\frac{C}{C_0} = kt \tag{3}$$

Where $C_0$ and $C$ are dye concentrations at time 0 (time to achieve an adsorption-desorption balance), and t, correspondingly, and $k$ is the rate constant ($min^{-1}$). The concentration decay of MB ($C/C_0$) of the prepared materials as a function of time is shown in figure 6(a). The kinetic curves of the $SnS_2$@$MoS_2$ against MB adopted the pseudo-second-order model, based on the value of $R^2$. Figure SI.2 shows the curves of the first order model. The rate of constants for $SnS_2$ and $SnS_2$@$MoS_2$ QDs can be evaluated from the data plotted in figure 6(b). Remarkably, $SnS_2$@$MoS_2$ QDs show superior photocatalytic activity for MB (figure 6(c)), where the degradation efficiency of $SnS_2$@$MoS_2$ QDs is approximately 2.7 and 0.43 times ($K = 20\,252\ min^{-1}$) higher than that for $SnS_2$ in 10 and 120 min ($K = 0.07506\ min^{-1}$), respectively, revealing the effect of $MoS_2$ QDs.

A schematic representative for the reaction mechanism of MB reduction by $SnS_2$@$MoS_2$ QDs nanocomposite under irradiation of visible light is demonstrated in figure 7. According to literature, the $MoS_2$ has a small energy gap and tends to metallic phase at around 1.7–1.9 eV and the Fermi energy of $MoS_2$ near to the valence band (VB), so $MoS_2$ is known to be a p-type semiconductor[43]. On otherwise the fermi level in $SnS_2$ lies close to the conduction band (CB); thus, $SnS_2$ is an n-type semiconductor. Based on the interface

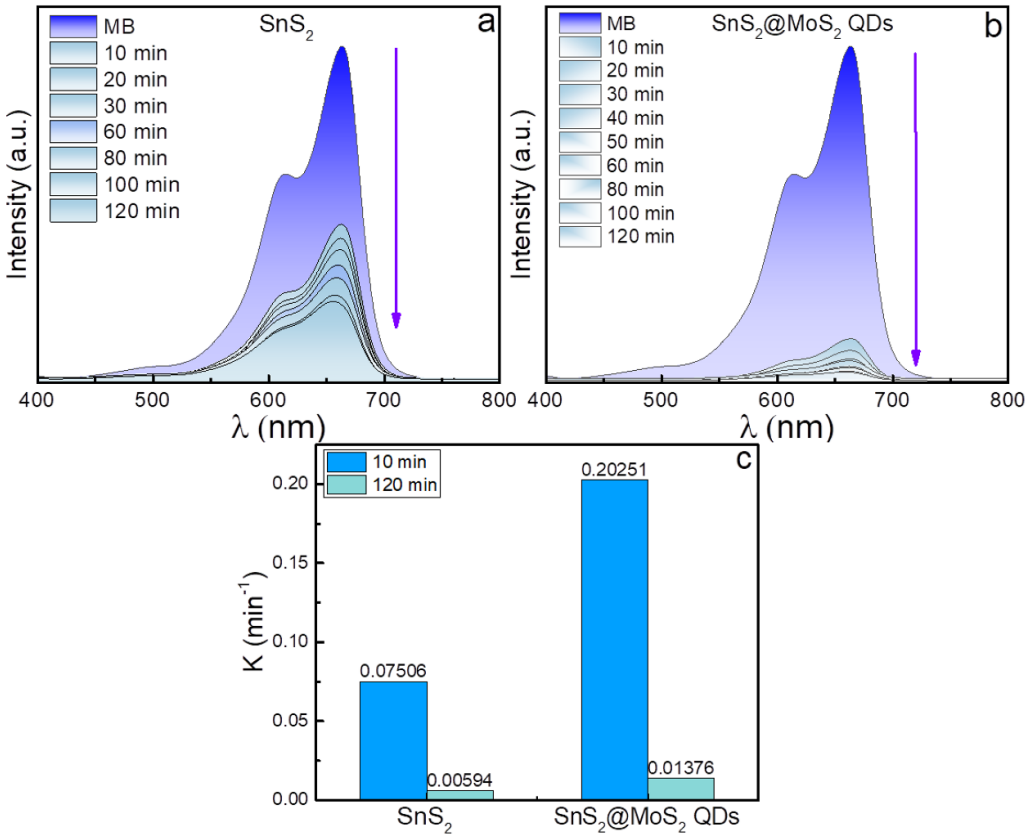


**Figure 5.** Absorption spectra of (a) $SnS_2$ and (b) $SnS_2$@$MoS_2$ and (c) Photodegradation efficiency of the prepared materials.

**Table 2.** Comparison of photocatalytic activity of $SnS_2$ based materials and our work.

| Catalyst | Dyes | Reaction time | Degradation rate (%) | Reference |
|---|---|---|---|---|
| Au/$SnS_2$ nanoflowers | MB | 60 min | 92.9% | [36] |
| $SnS_2$/$MoS_2$ | MB | 60 min | 58.0% | [14] |
| Cr doped $SnS_2$ | RhB | 120 min | 92.0% | [37] |
| $SnS_2$/RGO | RBB RBR | 150 min 150 min | ∼99.7% ∼ 97.0% | [17] |
| $SiO_2$@α-$Fe_2O_3$ | MB | 100 min | 99.0% | [38] |
| $SnS_2$-CdO | RhB CR | 210 min 210 min | 86.1% 92.8% | [39] |
| $ZnFe_2O_4$/SnS | MO | 120 min | 99.0% | [40] |
| CdS-SnS-$SnS_2$/rGO | ibuprofen | 120 min | 84.4% | [41] |
| $SnS_2$@$MoS_2$ QDs | MB | 10 min 120 min | 87.0% 98.0% | Our work |

among p-type $MoS_2$ and n-type $MoS_2$, a p-n junction is formed when the two junctions are connected, allowing the $MoS_2$ and $SnS_2$ Fermi energy ($E_f$) to increase and descend, respectively [44].

The photocatalytic reaction is occurred based on irradiating the $SnS_2$ @$MoS_2$ QDs by a source of light and both excited to produce pairs of $e^-$/h in accordance with equation (4) [43, 45, 46]:

$$SnS_2@MoS_2QDs + h\nu \rightarrow e^- + h^+ \quad (4)$$

Due to the more negative conduction band of $MoS_2$ than that of $SnS_2$, the photogenerated $e^-$ in the conduction band of $MoS_2$ transfer to the $SnS_2$ conduction band, while the $h^+$ photogenerated in the valence band of the $SnS_2$ might migrate to $MoS_2$, thus effectively separating $e^-$ and $h^+$ and consequently, increasing their lifetime before recombination. The small sizes of $MoS_2$ QDs can facilitate the electrons transition between $SnS_2$ and $MoS_2$ and provide more surface reaction sites for dye degradation. To avoid the recombination of $e^-$–$h^+$ pairs, significantly, the conduction band potential of $SnS_2$ became more negative enough to reduce the $O_2$ to produce the superoxide anion radical ($\cdot O^{2-}$) according to (equation (5)) [47].

$$O_2 + e^- \rightarrow \cdot O^{2-} \quad (5)$$

Moreover, the photogenerated holes in the valence band of the $SnS_2$ will move to the VB of $MoS_2$; interestingly, the $h^+$ residual in the $MoS_2$ VB will interact with water creating highly reactive hydroxyl radicals (.OH) and active oxidative power

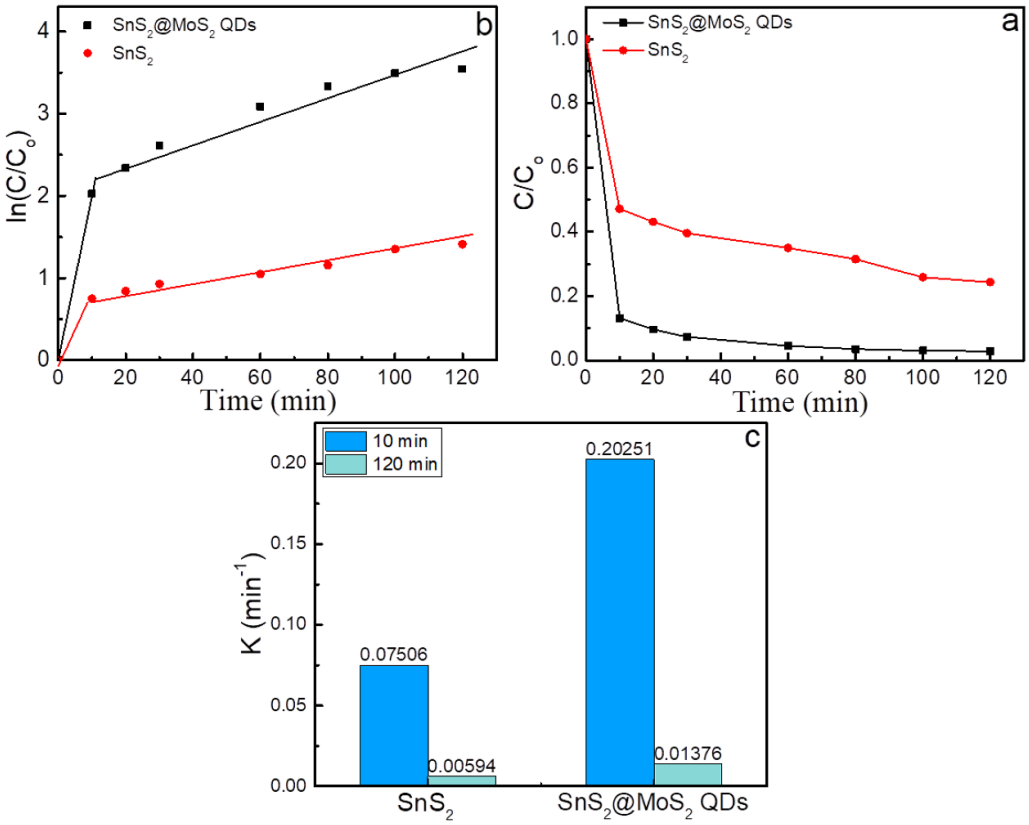


**Figure 6.** (a) Photodegradation efficiency ($C/C_0$) of the prepared materials, (b) Second-order kinetics mode corresponding equation (1) for MB, and (c) Constant reaction (K $min^{-1}$) of $SnS_2$ and $SnS_2$@$MoS_2$ QDs materials.

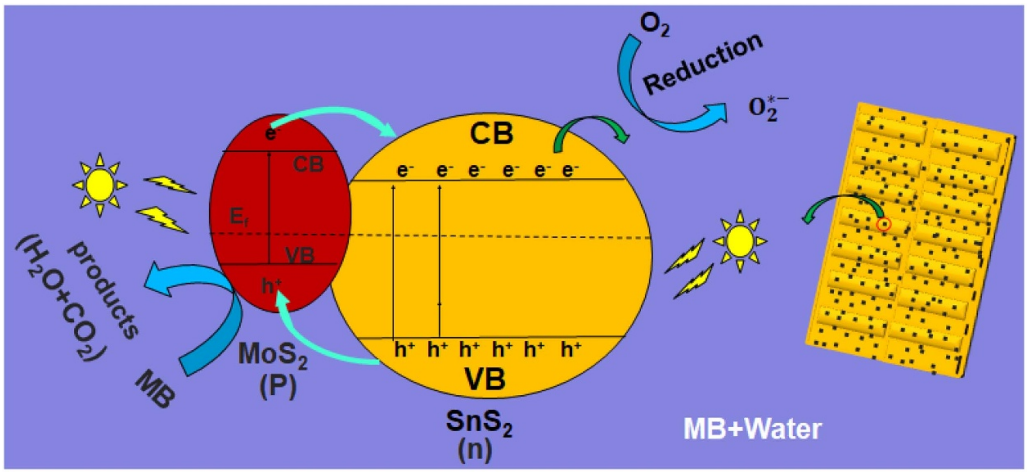


**Figure 7.** Schematic representation of the photocatalytic activity of $SnS_2$@$MoS_2$ QDs.

that could participate in the photocatalytic oxidation reaction. These reacting species result in degradation of MB dye (equation (6)).

$$MB + h^+ / \cdot O^{2-} \rightarrow Products(H_2O + CO_2) \qquad (6)$$

Consequently, this technique allowed the $SnS_2$@$MoS_2$ QDs photocatalysts to comprehend the highly efficient degradation of MB under the visible light irradiation.

## 4. Conclusion

In brief, $MoS_2$ QDs were prepared and then loaded on $SnS_2$ nanosheets via the ultrasonication technique for photocatalytic applications over MB. The XRD results confirmed that pure $SnS_2$ and $SnS_2$@$MoS_2$ QDs material have a single trigonal phase with space group P-3m1. The TEM images confirmed the formation of $SnS_2$@$MoS_2$ QDs nanocomposites with $MoS_2$ QDs size ranging from 5–7 nm. The UV–vis spectra proved an enhancement in the light absorption of $SnS_2$ after

coating by $MoS_2$, resulting in a decrease in the energy gap of $SnS_2$ after coating by $MoS_2$ QDs. Consequently, the photodegradation activity of $SnS_2$@$MoS_2$ QDs nanocomposites showed high performance toward MB compared to pure $SnS_2$. These results can be attributed to the strong light absorbance of the nanocomposite due to the construction of heterojunction between $SnS_2$ and $MoS_2$ QDs. Also, the good e−/h+ Paris separation in $SnS_2$@$MoS_2$ QDs nanocomposites, which confirmed by PL analysis, leads to high photocatalytic activity. This report successfully established a new structure with good heterojunction characteristics for photocatalytic applications. Therefore, according to this study, the optimization of $MoS_2$ QDs can open new window for future use of $MoS_2$ QDs basedhertostrcture in various applications.

## Acknowledgment

Research was financially supported by the Ministry of Science and Higher Education of the Russian Federation (State assignment in the field of scientific activity, № 0852-2020-0019)'

## ORCID iD

Gomaa Khabiri https://orcid.org/0000-0001-5993-4412

## References

[1] Song Y, Gu J, Xia K, Yi J, Chen H, She X, Chen Z, Ding C, Li H and Xu H 2019 *Appl. Surf. Sci.* **467** 56–64
[2] Zheng Y, Wang J, Wang Y, Zhou H, Pu Z, Yang Q and Huang W 2020 *Molecules* **25** 2
[3] Rani A, Singh K, Patel A S, Chakraborti A, Kumar S, Ghosh K and Sharma P 2020 *Chem. Phys. Lett.* **738** 136874
[4] Maniyam M N, Ibrahim A L and Cass A E 2020 *Environ. Technol.* **41** 71–85
[5] Türgay O, Ersöz G, Atalay S, Forss J and Welander U 2011 *Sep. Purif. Technol.* **79** 26–33
[6] Dong L, Li M, Zhang S, Si X, Bai Y and Zhang C 2020 *Desalination* **476** 114227
[7] Saber M R, Khabiri G, Maarouf A A, Ulbricht M and Khalil A S 2018 *RSC Adv.* **8** 26364–70
[8] Omar A M, Metwalli O I, Saber M R, Khabiri G, Ali M E, Hassen A, Khalil M M, Maarouf A A and Khalil A S 2019 Revealing the role of the 1T phase on the adsorption of organic dyes on $MoS_2$ nanosheets *RSC Adv.* **9** 28345–56
[9] Hu X, Cheng L and Li G 2017 *Mater. Lett.* **203** 77–80
[10] Cheng L, Hu X and Hao L 2018 *Ultrason. Sonochem.* **44** 137–45
[11] Voznyi A, Kosyak V, Opanasyuk A, Tirkusova N, Grase L, Medvids A and Mezinskis G 2016 *Mater. Chem. Phys.* **173** 52–61
[12] Wu Z, Xue Y, Zhang Y, Li J and Chen T 2015 *RSC Adv.* **5** 24640–8
[13] Zhang Y C, Li J, Zhang M and Dionysiou D D 2011 *Environ. Sci. Technol.* **45** 9324–31
[14] Zhang J, Huang G, Zeng J, Jiang X, Shi Y, Lin S, Chen X, Wang H, Kong Z and Xi J 2019 *J. Alloys Compd.* **775** 726–35
[15] Zhang Y C, Li J and Xu H Y 2012 *Appl. Catal.* B **123** 18–26
[16] Zhang Y C, Yao L, Zhang G, Dionysiou D D, Li J and Du X 2014 *Appl. Catal.* B **144** 730–8
[17] Dashairya L, Sharma M, Basu S and Saha P 2019 *J. Alloys Compd.* **774** 625–36
[18] Zhang Y C, Du Z N, Li K W and Zhang M 2011 *Sep. Purif. Technol.* **81** 101–7
[19] Lu D, Wang H, Zhao X, Kondamareddy K K, Ding J, Li C and Fang P 2017 *ACS Sustainable Chem. Eng.* **5** 1436–45
[20] Eda G, Fujita T, Yamaguchi H, Voiry D, Chen M and Chhowalla M 2012 *ACS Nano* **6** 7311–7
[21] Liang Z, Sun B, Xu X, Cui H and Tian J 2019 *Nanoscale* **11** 12266–74
[22] Li B, Jiang L, Li X, Ran P, Zuo P, Wang A, Qu L, Zhao Y, Cheng Z and Lu Y 2017 *Sci. Rep.* **7** 1–12
[23] Tan C, Luo Z, Chaturvedi A, Cai Y, Du Y, Gong Y, Huang Y, Lai Z, Zhang X and Zheng L 2018 *Adv. Mater.* **30** 1705509
[24] Sun J, Duan L, Wu Q and Yao W 2018 *Chem. Eng. J.* **332** 449–55
[25] Qiao W, Yan S, Song X, Zhang X, He X, Zhong W and Du Y 2015 *Appl. Surf. Sci.* **359** 130–6
[26] Tian X, Sun Y, Fan S, Boudreau M D, Chen C, Ge C and Yin -J-J 2019 *ACS Appl. Mater. Interfaces* **11** 4858–66
[27] Gu W, Yan Y, Zhang C, Ding C and Xian Y 2016 *ACS Appl. Mater. Interfaces* **8** 11272–9
[28] Liang Z, Guo Y, Xue Y, Cui H and Tian J 2019 *Mater. Chem. Front.* **3** 2032–40
[29] Yang M-Q, Han C and Xu Y-J 2015 *J. Phys. Chem.* C **119** 27234–46
[30] El Sayed A M and Khabiri G 2020 *J. Electron. Mater.* **49** 2381–92
[31] Qi Y, Xu Q, Wang Y, Yan B, Ren Y and Chen Z 2016 *ACS Nano* **10** 2903–9
[32] Liu Y, Li C-F, Li X-Y, Yu W-B, Dong W-D, Zhao H, Hu Z-Y, Deng Z, Wang C and Wu S-J 2019 *J. Colloid Interface Sci.* **551** 111–8
[33] Suganya M, Balu A, Anitha S, Prabha D, Balamurugan S, Priyanka B, Srivind J and Nagarethinam V 2018 *Mater. Sci. Eng.* B **229** 118–25
[34] Tan F, Qu S, Wu J, Liu K, Zhou S and Wang Z 2011 *Nanoscale Res. Lett.* **6** 1–8
[35] Yang Q, Tang K, Wang C, Zuo J, Zhang D and Qian Y 2003 *Thin Solid Films* **436** 203–7
[36] Feng J, Sun Y, Mu J, Chen L, Han T, Miao H, Liu E, Fan J and Hu X 2019 *Mater. Lett.* **236** 534–7
[37] Zhao W, Wei Z, Zhang L, Wu X and Wang X 2018 *Mater. Sci. Semicond. Process.* **88** 173–80
[38] Balu S, Uma K, Pan G-T, Yang T C-K and Ramaraj S K 2018 *Materials* **11** 1030
[39] Srivind J, Nagarethinam V, Suganya M, Balamurugan S, Prabha D and Balu A 2020 *Mater. Sci. Eng.* B **255** 114530
[40] Zhou J, Zhang Z, Kong X, He F, Zhao R, Wu R, Wei T, Wang L and Feng J 2020 *Appl. Surf. Sci.* **510** 145442
[41] Liang M, Yu Y, Wang Y and Yu Y 2020 *J. Hazard. Mater.* **391** 121016
[42] Cheng L, Yan J, Zhao S and Hao L 2019 *J. Alloys Compd.* **778** 924–32
[43] Dong R, Zhong Y, Chen D, Li N, Xu Q, Li H, He J and Lu J 2019 *J. Alloys Compd.* **784** 282–92
[44] Swain G, Sultana S, Moma J and Parida K 2018 *Inorg. Chem.* **57** 10059–10071
[45] Zhang L, Niu C-G, Wen X-J, Guo H, Zhao X-F, Liang C and Zeng G-M 2018 *J. Colloid Interface Sci.* **532** 557–570
[46] Zhang G, Chen D, Li N, Xu Q, Li H, He J and Lu J 2018 *J. Colloid Interface Sci.* **514** 306–315
[47] Wang X, Hong M, Zhang F, Zhuang Z and Yu Y 2016 *ACS Sustainable Chem. Eng.* **4** 4055–63